Effects of synthetic parameters on the catalytic performance of Au/CeO<inf>2</inf> for furfural oxidative esterification

Effects of synthetic parameters on the catalytic performances of Au/CeO_2 catalysts for furfural oxidative esterification

Maela Manzoli[a*], Federica Menegazzo[b], Michela Signoretto[b], Giuseppe Cruciani[c], Francesco Pinna[b]

[a] *Department of Chemistry & NIS Interdepartmental Centre, University of Turin, Via P. Giuria 7, 10125 Turin, Italy*

[b] *Department of Molecular Sciences and Nanosystems, Ca' Foscari University of Venice and INSTM-RU Ve, Dorsoduro 2137, 30123 Venice, Italy*

[c] *Department of Physics and Hearth Science, University of Ferrara, Via Saragat 1, 44122 Ferrara, Italy*

*Corresponding author:

Dr. Maela Manzoli,

maela.manzoli@unito.it

phone number: +39 011 6707541

Abstract

The synthetic parameters affecting the Au/CeO_2 catalytic performances in furfural oxidative esterification were investigated. Thermal analysis (TG/DTA), N_2 adsorption/desorption, X-ray powder diffraction (XRD), high resolution transmission microscopy (HRTEM), CO pulse chemisorption, diffuse reflectance UV–Vis and

transmission FTIR spectroscopies were employed to study the role of different ceria supports on the nature of the gold species and on the catalytic activity. Unexpectedly, the larger is the gold size, the higher is the activity, whilst no influence on the selectivity to methyl-2-furoate has been observed. Lower amounts of carbonate species and more coordinated Ce^{4+} sites at the surface of the most active catalyst calcined at 500 °C can explain the enhanced activity. A clean surface is directly related to the ceria capability to provide activated oxygen. Reverse oxygen spillover can occur at the perimeter of the Au nanoparticles and that these gold sites could be involved in the activation of methanol.

Key words: gold catalyst; Au; CeO_2; support; deposition-precipitation; furfural, oxidation; esterification; biomass.

Introduction

Oxidation is a key reaction in organic synthesis and will likely play a significant role in the development of value-added chemicals from biomass. The application of heterogeneous catalysis and molecular oxygen to oxidation reactions offers a green alternative to traditional, toxic chemical oxidants. The potential for biomass valorization in the framework of biorefineries is enormous. However, successfully replacing petroleum based fuels and chemicals with biomass-based products of lignocellulose will require high-yield, low-cost and energetically efficient targeted upgrading processes.

Dehydratation of C6 and C5 biomass sugars under mineral acid solutions leads to the formation of furans compounds including furfural (2-FA) and hydroxymethylfurfural. The two compounds have a very high platform potential for chemical production in biorefineries. For example, oxidation of furfural allows production of relevant carboxylic acids, such as furoic and maleic acids [1]. By furfural oxidative esterification it is possible to obtain methyl-2-furoate, which is used as flavor and fragrance component and is a higher added value product. Christensen et al. have firstly investigated furfural oxidative esterification using a commercial Au/TiO_2 catalyst by the World Gold Council in the presence of a base (8% CH_3ONa) [2]. Subsequently Corma et al. studied the same reaction using gold based catalysts, but avoiding the use of the base, that would make the process less green and less advantageous from an economic point of view [3]. We have extensively investigated gold based catalysts on different supports for a base free esterification of furfural [4-6]. Very recently, we verified the real mechanism of the furfural oxidative esterification with gold on zirconia catalyst under our reaction conditions and identified the best process conditions in terms of pressure, temperature, nature of the oxidizing agent and reaction time, in order to yield

the process greener, safer, economic and sustainable [7]. From literature studies, it is possible to say that the choice of gold nanoparticles is advantageous for oxidative esterification reactions, but it is necessary to improve the performances of the catalyst in order to make the process industrially feasible.

Cerium oxide is a rare earth oxide that has received a great deal of interest from researchers because of its unusual properties includes high chemical stability, high charge transfer capability, non-toxicity oxygen ion conductivity, and biocompatibility [8]. Cerium has two stable oxidation states, +4 and +3, and the relatively ease of switching between these two states is the essential factor for its catalytic activity. This rapid change of oxidation state is related to its ability to store and release oxygen, a property measured by the ‘‘oxygen storage capacity’’ (OSC) [9]. These characteristics make CeO_2 a very interesting support for oxidation reactions [10 and references therein].

Therefore, the study of an efficient Au/CeO_2 catalytic system able to operate without the presence of a base, which negatively affects the sustainability of the 2-FA oxidative esterification reaction is here reported. The goal of the present work is to investigate the effect of the different calcination temperature to which the support and the final catalysts were submitted on both Au size and ceria support and to check the role of such features on the conversion and the selectivity in the esterification reaction.

2. Experimental

2.1 Synthesis of the supports

Ceria supports were synthesized by precipitation from $(NH_4)_2Ce(NO_3)_6$ by urea in aqueous solution [11, 12]. The solution was stirred and boiled at 100 °C for 6 h, the

precipitate was washed twice in boiling deionized water and dried at 110 °C for 15 h (Ce110). Part of this material was calcined at 300 °C (Ce300) and part at 500 °C (Ce500) in flowing air (50 mL/min) for 3 hours.

As for the Ce90 support, the solution was mixed and boiled at 90 °C, immediately filtered, washed twice in boiling deionized water and dried at room temperature (r.t.).

2.2 Preparation of the catalysts by gold deposition-precipitation (dp)

1.5 wt% of gold was added by deposition-precipitation (dp) at pH=8.6: the supports were suspended in an aqueous solution of $HAuCl_4 \cdot 3H_2O$ for 3 hours and the pH was controlled by the addition of NaOH (0,5 M). After filtration the samples were dried at 35 °C for 15 h and finally calcined in air for 1 hour at 300 °C or 500 °C. The obtained samples will be hereafter denoted as Ce90Au300, Ce90Au500, Ce110Au300, Ce110Au500, Ce300Au300 and Ce500Au500, respectively.

2.4 Methods

Thermal analyses (TG/DTA) were performed on a NETZSCH STA 409 PC/PG instrument in flowing air (20 mL/min) with temperature rate set at 5 °C/min in the 25-900 °C temperature range.

Surface areas and pore size distributions were obtained from N_2 adsorption/desorption isotherms at -196 °C (using a Micromeritics ASAP 2000 analyser). Surface areas were calculated from the N_2 adsorption isotherms by the BET equation, and pore size distribution were determined by the BJH method [13]. Total pore volumes were taken at $p/p_0 = 0.99$.

The gold amount of both fresh and exhausted catalysts was determined by atomic absorption spectroscopy (AAS) after microwave disgregation of the samples (100 mg) using a Perkin-Elmer Analyst 100.

X-ray powder diffraction (XRD) patterns were measured by a Bruker D8 Advance diffractometer equipped with a Si(Li) solid state detector (SOL-X) and a sealed tube providing Cu K_α radiation. Measuring conditions were 40 kV x 40 mA. Apertures of divergence, receiving and detector slits were 1°, 1°, and 0.3° respectively. Data scans were performed in the 2θ ranges 15-55° and 35-40° with 0.02° step size and counting times of 3 s/step and 10 s/step, respectively.

High resolution transmission microscopy (HRTEM) measurements were performed using a side entry Jeol JEM 3010 (300 kV) microscope equipped with a LaB_6 filament and fitted with X-ray EDS analysis by a Link ISIS 200 detector. For analyses, the powdered samples were deposited on a copper grid, coated with a porous carbon film. All digital micrographs were acquired by an Ultrascan 1000 camera and the images were processed by Gatan digital micrograph. A statistically representative number of particles was counted in order to obtain the particle size distribution. The mean particle diameter (d_m) was calculated as $d_m = \Sigma d_i n_i / \Sigma n_i$, where n_i was the number of particles of diameter d_i.

Diffuse reflectance UV–Vis-NIR analysis was performed on the samples in the form of powders. The as prepared samples were placed in a quartz cell, allowing treatments in controlled atmosphere and temperature, but spectra recording only at r.t.. Diffuse reflectance UV–Vis-NIR spectra were run at r.t. on a Varian Cary 5000 spectrophotometer, working in the range of wavenumbers 190-2500 nm. UV–Vis-NIR

spectra are reported in the Kubelka-Munk function [$f(R\infty)=(1-R\infty)2/2R\infty$; $R\infty$=reflectance of an "infinitely thick" layer of the sample.

CO pulse chemisorption measurements were performed at -116 °C in a lab-made equipment. Before the analyses, the following pre-treatment was performed: the sample (200 mg) was reduced in a H_2 flow (40 ml/min) at 150 °C for 60 min, cooled in H_2 to r.t., purged in He flow and finally hydrated at r.t.. The hydration treatment was performed by contacting the sample with a He flow (10 ml/min) saturated with a proper amount of water. The sample was then cooled in He flow to the temperature chosen for CO chemisorption (-116 °C) [14].

The surface of the Au catalysts has been characterized by means of transmission FTIR measurements, performed on the samples in self-supporting pellets introduced in a cell allowing thermal treatments in controlled atmospheres and spectrum scanning at controlled temperatures (from -196 °C to 25 °C). The FTIR spectra were taken on a Perkin Elmer 2000 spectrometer (equipped with a cryogenic MCT detector). The activation pre-treatments to which the samples were submitted before the measurements were i) outgassing at r.t.; ii) oxidation in O_2 either at 300 °C or at 500 °C in order to clean the surface from carbonate species and water. Such species are present due to the exposition to air. The thermal treatment consisted of i) outgassing from r.t up to 200 °C, ii) from 200 °C to 300 °C or 500 °C in O_2 (25 mbar); iii) 30 min at 300 °C or 500 °C in O_2 (25 mbar, changed every 10 min); iv) cooled to r.t. in oxygen atmosphere. The spectra were normalised respect to the weight of the pellets and to the effective gold content, the latter is reported in Table 1. In the case of the methanol adsorption experiment, the spectrum of the sample before the inlet of CH_3OH was subtracted from each spectrum.

2.5 Catalytic activity measurements

2-FA oxidative esterification with oxygen and methanol was investigated at 120 °C, without $NaCH_3O$ addition, using a mechanical stirred autoclave fitted with an external jacket [6]. Catalyst (100 mg), 2-FA (Sigma Aldrich, ›99%; 300 μL) and n-octane (Sigma Aldrich, ›99%; 150 μL), used as internal standard, were added to the solvent (150 mL of methanol). The reactor was charged with oxygen (6 bar) and stirred at 1000 rpm. The progress of the reaction was determined after 90 min by gas-chromatographic analysis of the converted mixture (capillary column HP-5, FID detector).

3. Results and Discussion

3.1 Preliminary characterization of the supports

Firstly, one ceria support was synthesized according to the procedure reported in the literature [11] and simply dried it at 110 °C (Ce110). A thermal TG/DTA analysis (Figure 1) was carried out in order to have information on the behavior of the material during calcination starting from room temperature up to 900 °C in O_2 atmosphere.

The TG curve indicates that the sample underwent to a weight loss between 50 and 200 °C, corresponding to 4 wt%. In correspondence to this weight loss there is a large endothermic peak in the DTA curve, due to the release of water from the surface of the ceria support. Then the TG profile slowly decreases of about 2 wt% until 800 °C, while DTA curve shows an exothermic band that can be reasonably ascribed to carbonate and nitrate compounds. Indeed, the precursor of ceria is $(NH_4)_2Ce(NO_3)_6$, and it is well known that ceria is inclined to absorb CO_2 from atmosphere.

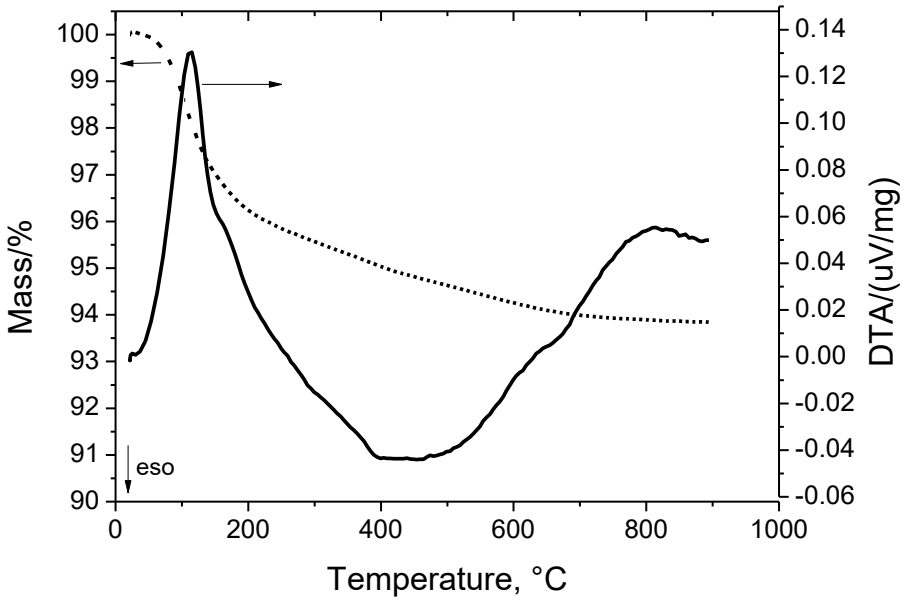

Figure 1: TG-DTA analysis of the Ce110 support.

Basing on the TG/DTA results, we chose to perform the calcination of the sample at 300 °C and at 500 °C to obtain supports completely or partially free from residual species left at the surface of the ceria support during the decomposition the Ce precursor, which can behave as poison during the reaction. There is no apparent evidence for ceria phase transition on the TG-DTA profile and the global weight loss is only 6 wt%. Such value is very low if compared to a 40 wt% weight loss reported previously for $Ce(OH)_4$ [15]. We can suppose that in our experimental conditions crystalline CeO_2, and not the expected $Ce(OH)_4$, is directly precipitated. In order to confirm our hypothesis, we prepared another support performing the synthesis at 90 °C. In this case, the aging was stopped immediately after precipitation.

The structure of the four supports was investigated by X-ray diffraction and the obtained patterns are shown in Figure 2 in the 2θ region between 15 and 70. Firstly, it

can be noted that the spectra related to Ce100, Ce300 and Ce500 are indistinguishable among each other.

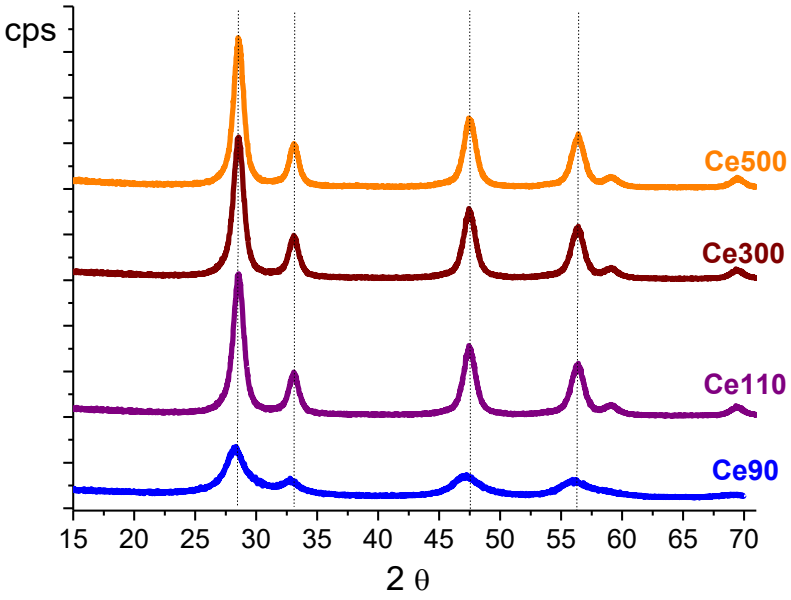

Figure 2: XRD patterns of the different ceria supports.

The peaks observed at 2 theta 28, 37, 47.5, 56, 59 and 69 can be assigned to (111), (200), (220), (311), (222) and (400) peaks, respectively of cubic CeO_2 (cerianite-(Ce), syn; file number 00-034-0394). This finding is in agreement with the TG-DTA analysis, suggesting that the calcination is not necessary for the formation of crystalline CeO_2. Moreover, some authors have supposed that the chemical formulation of $Ce(OH)_4$ is probably incorrect and the material is really a disordered hydrous cerium oxide [16].

If compared to the other spectra, the Ce90 pattern shows a larger peak width and the peaks are shifted to lower 2 θ. These features can indicate the presence of very small CeO_2 nanoparticles. On the other hand, the larger cell could be due to the presence of OH groups, indicating $Ce(OH)_4$ as defective CeO_2 type structure in agreement with our previous hypothesis [16].

3.2 Catalytic activity and characterization of the catalysts

Gold was then introduced by dp on the supports to investigate how the support rules the gold dispersion and then the catalytic activity. The catalysts were tested in the 2-FA oxidative esterification to methyl-2-furoate (see Scheme 1).

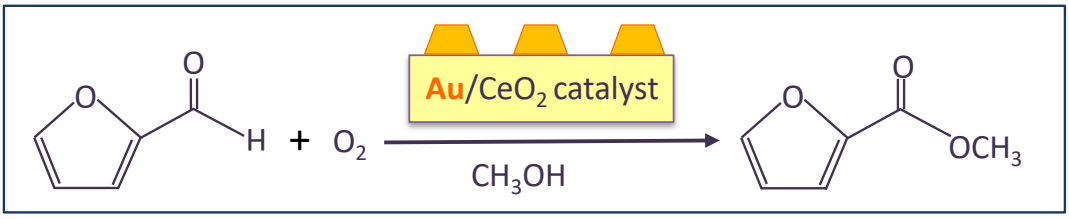

Scheme 1: 2-FA oxidative esterification to methyl-2-furoate.

Such reaction was carried out in methanol without the addition of $NaCH_3O$, which would make the process less green and more expensive [3]. Moreover, mild reaction conditions, comparable to those reported in the literature [3], were employed (120 °C and 6 bar).

In Figure 3 the conversions obtained after 90 minutes of reaction are shown. Selectivity to methyl-2-furoate is 100% for all the samples (data not shown), in agreement with our previous FTIR characterization, that confirmed that the formation of the product seems to occur without generation of any adsorbed intermediate species and that the reaction proceeds through direct selective oxidation of furfural to the desired furoate [7].

With regard to conversions, there is clear indication that the calcination of the support is a key step in the synthetic procedure. The higher is the calcination temperature of the support, the higher is the catalytic activity. This is true for both series

of samples re-calcined at 300 °C or 500 °C after gold introduction. Moreover, the two catalysts supported on Ce90 show very low conversion. These observations make the Ce90 support not suitable for the preparation of active gold catalysts, further confirming that it is necessary to use crystalline CeO_2 nanoparticles as support.

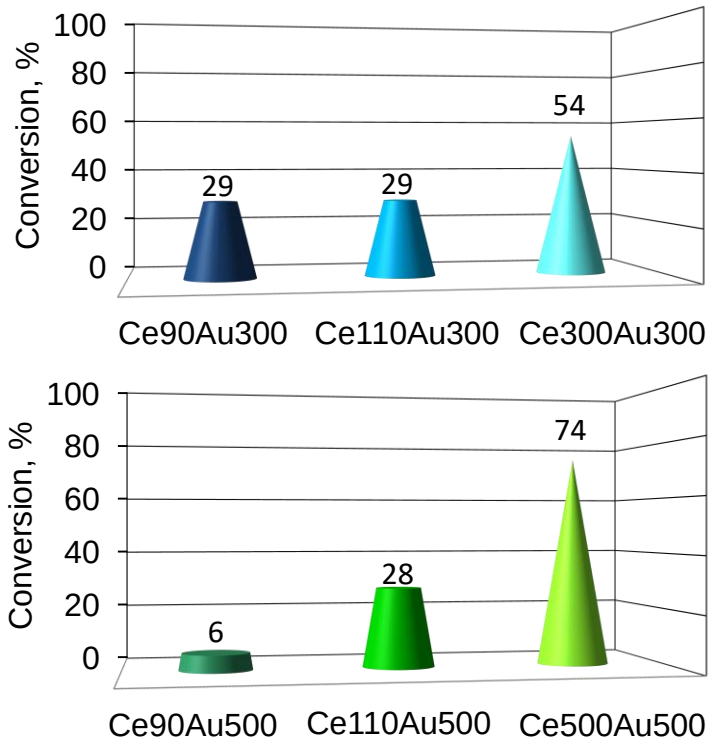

Figure 3: Catalytic performances in the 2-FA oxidative esterification reaction of the examined samples. Selectivity is 100% for all catalysts. (at 120 °C - 6 bar O_2 – 90 min of reaction).

The best performing catalyst is the one supported on ceria submitted to calcination at 500 °C. The catalyst prepared by using this support and re-calcined at 500 °C after gold introduction presents the highest conversion. In order to explain the differences observed among the catalysts and to understand the role of the support, a detailed

characterization has been performed to highlight the parameters that control the catalytic activity in the oxidative esterification of furfural.

In Table 1 the effective gold content of the catalysts prepared by dp is reported. The samples supported on Ce110, Ce300 and Ce500 exhibit an effective gold content which is quite similar to the nominal one. On the contrary, the gold amount is higher than the nominal content for the two catalysts supported on Ce90. This is reasonably ascribable to the presence of water on the support, due to the drying at room temperature.

Table 1: Characterization data of the catalysts.

Sample	Au nominal content (wt%)	Au effective content (wt%)	Surface area (m^2/g)	Mean pore size (nm)
Ce90Au300	1.5	2.1	180	3.1
Ce90Au500	1.5	2.1	105	3.2
Ce110Au300	1.5	1.3	121	7.7
Ce110Au500	1.5	1.3	121	7.9
Ce300Au300	1.5	1.4	124	7.7
Ce500Au500	1.5	1.5	110	8.4

Then N_2 physisorption analyses were carried out to determine the surface area and pore size distribution of the catalysts. This point is crucial since the choice of an appropriate mesoporous material can rule out mass transfer problems and at the same time can allow a good dispersion of the Au active phase. The adsorption isotherms of the samples, as well as their BJH pore size distributions, are shown in Figure 4, while the corresponding values are reported in Table 1.

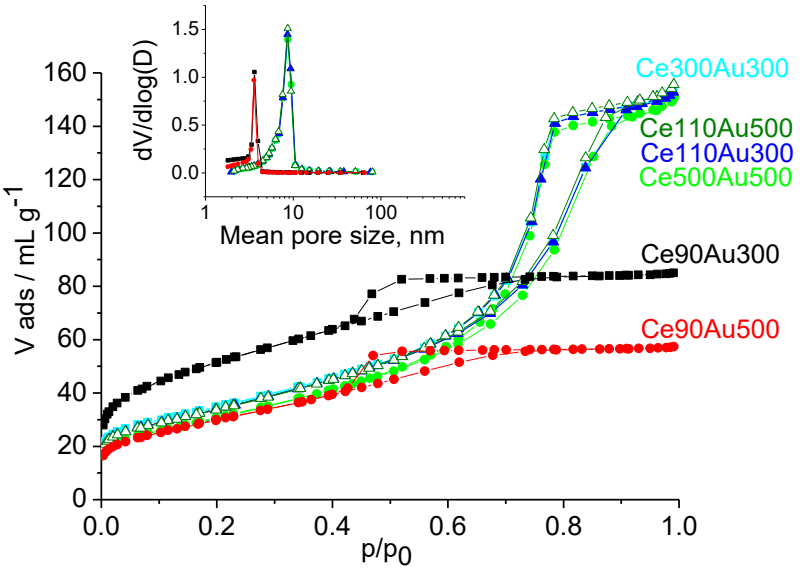

Figure 4: N_2 physisorption isotherms of the catalysts and BHJ pore size distributions (insert).

All samples exhibit type IV isotherms with a hysteresis loop typical of mesoporous materials, moreover unimodal pore distributions have been obtained. As summarized in Table 1, the surface area (ranging from 124 to 110 m^2/g) and the mean pore size (ranging from 7.7 to 8.4 nm) are similar for the samples supported on Ce110, Ce300 and Ce500. If compared to the other samples, Ce90Au300 and Ce90Au500 behave completely different, since the adsorption isotherms are at a lower relative pressure (from 0.4 to 0.7 p/p_0) and the mean pore sizes are significantly lower than the other distributions. These features indicate that Ce90 does not possess adequate textural properties to be employed as a support and further confirm our previous findings.

Figure 5 shows the XRD patterns of the catalysts. The structure of ceria is mantained after Au dp and subsequent calcination, as indicated by the presence of almost the same XRD peaks observed in the case of the corresponding supports (see also Figure 2).

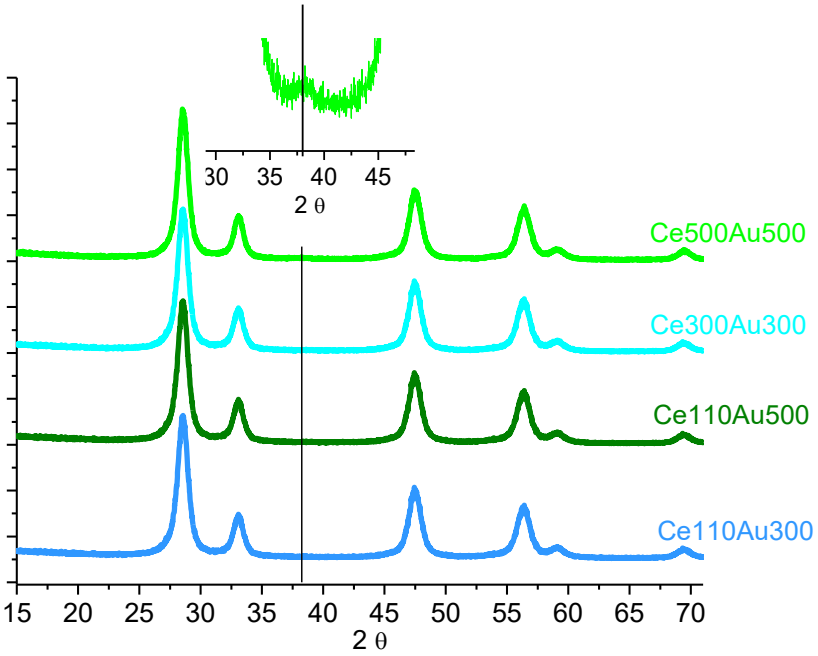

Figure 5: X-ray diffraction patterns of the catalysts prepared by dp. Inset: zoom of the XRD pattern of Ce500Au500 in the 30-45 2 θ range.

The expected diffraction peaks associated with the presence of crystalline gold should appear at 38.1°, 44.3°, 64.5°, 77.6° and 81.6° corresponding to the (111), (200), (220), (311) and (222) faces of the cubic structure [file number 4-0784, 17].

Notably, a very weak and broad peak at 2 theta 38.1 (see inset), corresponding to crystalline gold has been detected only the Ce500Au500 catalyst, that is the sample calcined at the highest temperature. Rietveld analysis of the peak related to gold reveals that it can be fitted with a crystal size (LVol-IB) of about 2 nm and a 2 wt % Au amount has been obtained. No peaks ascribable to crystalline Au have been detected for the other three catalysts. Such absence might be related to the presence of highly dispersed gold nanoparticles on ceria.

A careful HRTEM analysis has been carried out on the Ce110Au500 and Ce500Au500 samples to explore the effect of the calcination at 500°C on the most active catalyst and the results are summarized in Figure 6.

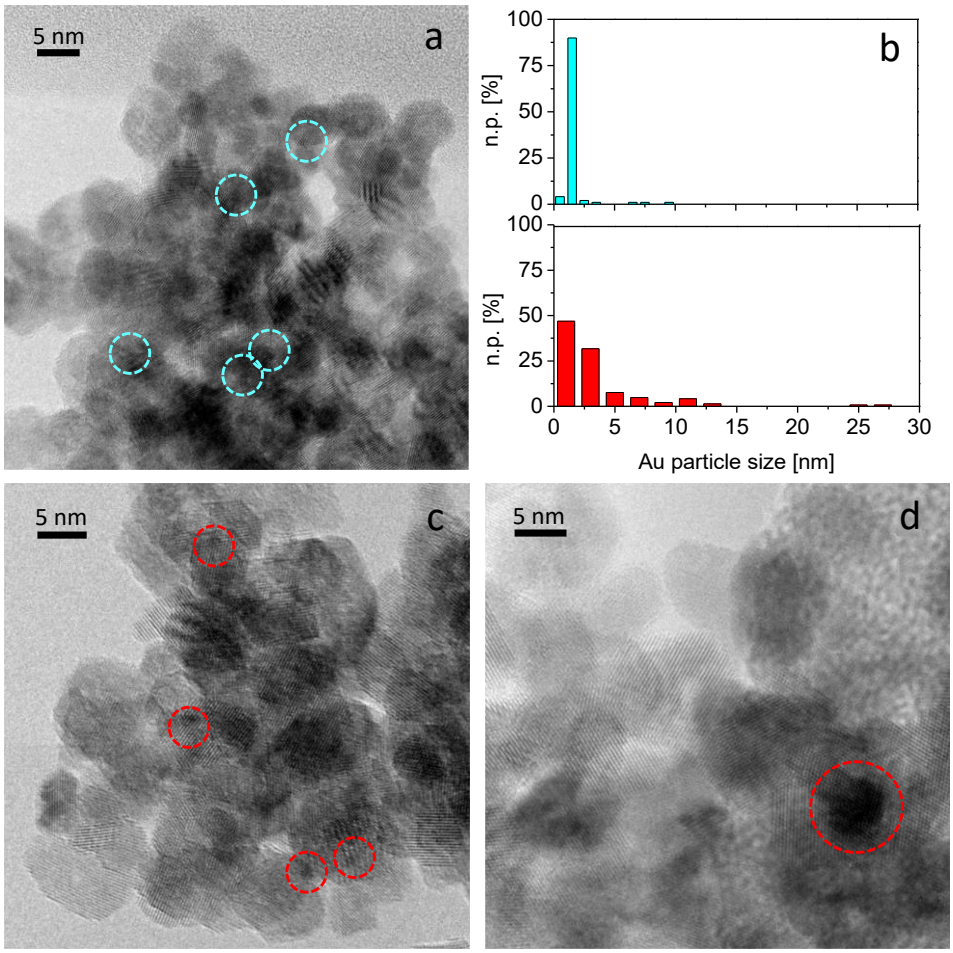

Figure 6: HRTEM images collected on Ce110Au500 (section a) and Ce500Au500 (sections c and d): roundish Au nanoparticles with different size are signaled by cyan and red circles, respectively. The Au particle size distributions of Ce110Au500 (cyan) and Ce500Au500 (red) are reported and compared in section b. Instrumental magnification: 300000X, 400000X and 500000X, respectively.

Roundish gold nanoparticles have been observed either on Ce110Au500 (section a) or on Ce500Au500 (sections c and d). The particle size distribution of Ce110Au500 indicates that the majority of the gold species has size around 2 nm, being the average size equal to 2.5 ± 1.2 nm (section c). The calcination at 500 °C to which the Ce110 support was submitted before gold dp affected the metal dispersion, indeed the gold dispersion is lower (see section d of Figure 6) as indicated by the broader particle size distribution (section b of the same figure). The average size obtained for the Ce500Au500 catalyst is 3.4 ± 1.3 nm, in quite good agreement with XRD findings.

UV-Vis diffuse reflectance (DRUV-Vis) spectroscopy was employed to more deeply investigate the nature of the gold species. The ceria support is a pale yellow powder and absorption bands at about 235, 267 and 338 nm due to the intrinsic band-gap absorptions of CeO_2 nanoparticles have been observed for all samples. The maxima at 267 amd 338 nm can be assigned to the electron transitions from the valence band to the conduction band (O(2p) to Ce (4f) and to interband transitions, respectively. The maximum at 235 nm is most likely due to $Ce^{3+} \leftarrow O_2^-$ charge transfer [18-21] (data not shown for the sake of brevity). The DRUV-Vis spectra of the as prepared samples are reported in Figure 7 in the 400-1500 nm region, in order to focus on the plasmonic absorption of gold.

All the as prepared Au catalysts show a typical plasmonic absorption in the wavelength range of 500-950 nm, due to the presence of gold nanoparticles [22-25]. However, looking at the spectra, it can be observed that the maxima slightly differ as for the position and above all that the bands have different intensity.

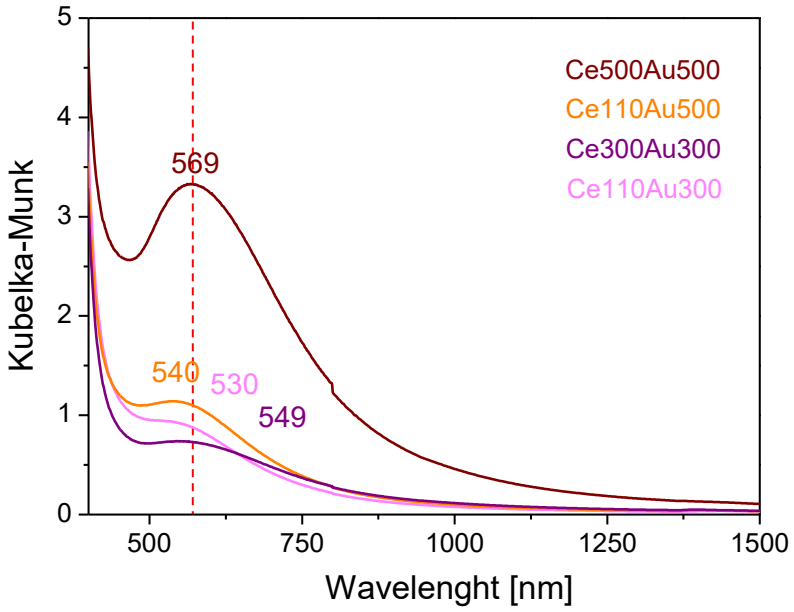

Figure 7: DRUV-Vis spectra of the as prepared samples supported on ceria.

The positions of the maxima as well as the observed shifts (referred to the position of the maximum related to the sample calcined at the lowest temperature, namely Ce110Au300) are reported in Table 2.

Table 2: DRUV-Vis and CO chemisorption data of the catalysts

Sample	Position of the Au plasmonic band (nm)	Observed shift (nm)*	mol_{CO}/mol_{Au}
Ce110Au300	530	-	0.1
Ce110Au500	540	10	0.05
Ce300Au300	549	19	0.18
Ce500Au500	569	39	0.08

* the shift were evaluated by referring to the position of the plamonic band at 530 nm.

More in detail, an increase in intensity of the plasmonic absorption as well as a red shift of the maxima position occurred by increasing the temperature of calcination, i.e. when the Ce110 support is calcined either at 300 °C or at 500 °C before the deposition-precipitation of gold. This effect is particularly evident in the case of Ce500Au500, that shows the most intense and red shifted plasmonic absorption at 569 nm, indicating that on this sample the metal dispersion is lower than that of the other samples, in agreement with the previous XRD and HRTEM findings.

The shape of the plasmonic bands related to Ce300Au300 and Ce500Au500 is broader than that of the corresponding not calcined samples, Ce110Au500 and Ce110Au300. This feature further indicates a role of the final calcination to which the catalysts underwent on the gold size. Moreover, DRUV-Vis results are supported by CO chemisorption analyses, carried out to evaluate the gold dispersion of all samples. The CO chemisorption is reported as mol_{CO}/mol_{Au} ratio, because it gives an indication of the number of uncoordinated gold sites able to absorb CO. These uncoordinated sites can be also involved in oxygen activation and the above ratio allows to compare directly all samples, since it refers to the number of moles of Au in each sample. As a consequence, CO chemisorption gives also a measure of gold dispersion [14]. CO chemisorption put in evidence a decrease of the mol_{CO}/mol_{Au} ratio by increasing the temperature of calcination, as summarized in Table 2. In addition, a comparison among the mol_{CO}/mol_{Au} obtained values (reported in Table 2) and the corresponding conversions in the 2-FA oxidative esterification for the catalysts supported on Ce90, Ce110, Ce300 and Ce500 submitted to a final calcination at 300°C or at 500°C (upper and lower panels of Figure 3, respectively) was performed. As for the catalysts finally calcined at the same

temperature, the data firstly indicate that the higher is the gold dispersion, the higher is the conversion on the sample. However, a decrease of the gold dispersion accompanied by an increase in the conversion is observed by raising the calcination temperature from 300°C up to 500°C. The comparison between the two more promising catalysts, i.e. Ce300Au300 and Ce500Au500, reveals a controlled drop from 0.18 mol_{CO}/mol_{Au} to 0.08 mol_{CO}/mol_{Au} against an enhancement of the conversion (from 54% up to 74%).

3.3 Role of the calcination temperature of the support on the nature of gold species and on the catalytic activity

DRUV-Vis analyses as well as CO chemisorption results clearly indicated that the calcination temperature to which the ceria underwent before gold dp strongly affects the support as well as the final catalysts, resulting in the formation of gold nanoparticles with a greater size. Moreover, with the exception of Ce90, XRD measurements performed on the supports calcined at different temperature confirm that both structure and size of the obtained ceria did not change either by increasing the temperature or by introducing gold and performing the second calcination.

The CeO_2 particle size distributions of Ce110Au500 (orange) and Ce500Au500 (purple) obtained by HRTEM measurements are compared in Figure 8.

The aim is to further put in evidence possible effects of performing the calcination at 500°C, that is the temperature which produced the most active catalyst. The calculated average diameter of ceria for Ce110Au500 is 6.3 ± 1.6 nm and for Ce500Au500 is 6.4 ± 1.2 nm. The obtained values are very similar and in addition no substantial differences in the particle size distribution are evident. However, some changes do effectively occur on ceria, because the catalysts bear different Au species with different size. Therefore,

there should be a change located at the surface of the oxide that is able to influence the deposition of the metal.

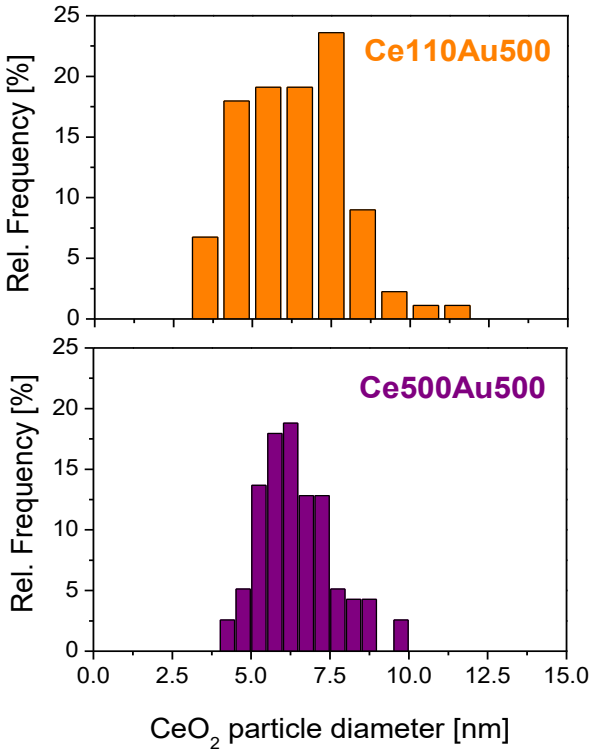

Figure 8: CeO_2 particle size distributions of Ce110Au500 (orange) and Ce500Au500 (purple).

FTIR spectroscopy measurements were carried out to characterize the surface of both Ce300Au300 and Ce500Au500 catalysts. The goal was to point out the occurrence of discrepancies that can be correlated to the different catalytic activity displayed by the two samples. The comparison between the FTIR absorbance spectra of Ce300Au300 and Ce500Au500 simply outgassed at r.t. 30' and after oxidation at 300 °C and 500 °C is shown in the 1750-800 cm^{-1} region in Figure 9, section a and section b, respectively.

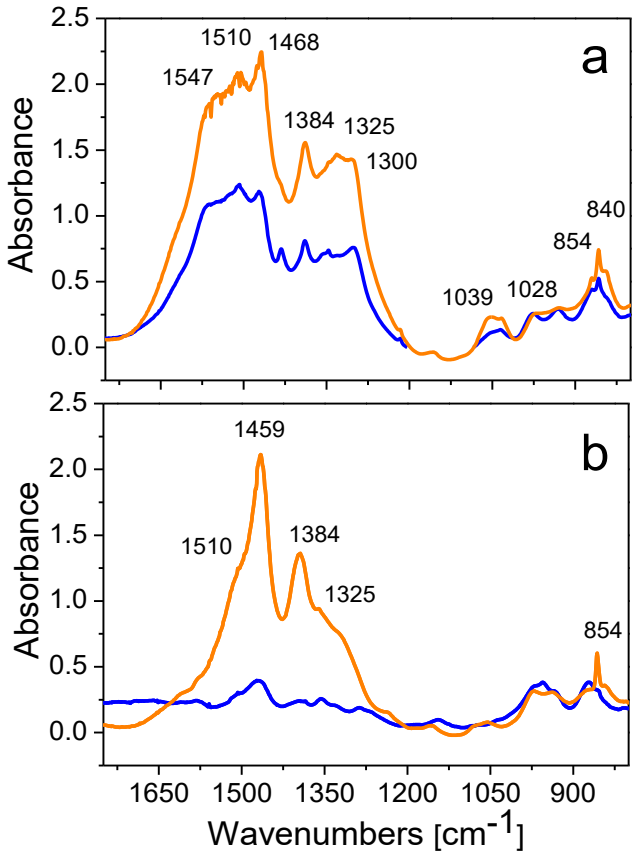

Figure 9: FTIR absorbance spectra of Ce300Au300 (orange curves) and Ce500Au500 (blue curves) outgassed at r.t. 30' (section a) and after oxidation at 300 °C and 500 °C, respectively (section b).

The FTIR spectra clearly indicate that different carbonate species (monodentate species, bands at 1510 and 1325 cm^{-1}; bidentate species, bands at 1547, 1300, 1028 and 840 cm^{-1}; and polydentate species, bands at 1468, 1384, 1039 and 854 cm^{-1} [26]) are present at the surface of both samples simply outgassed at room temperature (section a). Moreover, the intensity of these bands is higher in the case of Ce300Au300.

The spectra collected after thermal treatment in oxygen at 300 °C and at 500 °C are reported in section b of the same figure. In both cases, the oxidation induces a decrease

in the amount of carbonate species; however, the decrease is significantly larger after oxidation at 500°C, indicating that the surface of the Ce500Au500 catalyst is more free from adsorbed carbonate species.

The subsequent inlet of methanol at r.t. on Ce300Au300 and Ce500Au500 produced comparable amounts of different methoxy species, as showed in Figure 10, where the FTIR difference spectra collected on the two samples in the 950-1150 cm^{-1} region upon adsorption of 5 mbar CH_3OH are shown.

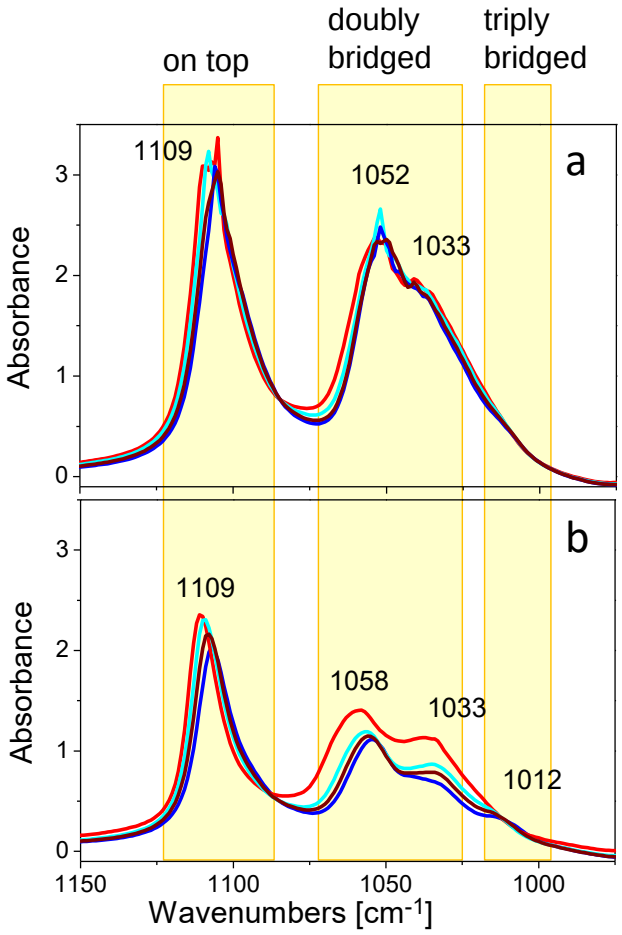

Figure 10. FTIR difference spectra collected on Ce300Au300 (section a) and Ce500Au500 (section b) upon the inlet of 5 mbar CH_3OH (red curves) and under outgassing at r.t. after 1' (cyan curves), after 10 min (brown curves), after 30' (blue curves).

On top (band at 1109 cm^{-1}) and doubly bridged (bands at 1052-1058 and 1033 cm^{-1}) methoxy species have been detected on both samples [27, 28], whereas on Ce500Au500 also triply bridged methoxy species are present [27, 28], further confirming the higher degree of cleanliness of the surface of the sample calcined at a higher temperature. However, the most interesting feature is the behavior of the bands towards the outgassing at r.t., that indicates that methoxy species are less stable on the surface of Ce500Au500. Such behavior can indicate a more easy activation of methanol and an enhanced reactivity of methoxy species on this sample, in agreement with the catalytic activity results.

CO adsorption experiments at 90 K were performed to probe and to compare the nature of the surface sites present on Ce300Au300 and Ce500Au500 after thermal treatment in oxygen at 300 °C and 500 °C, respectively. The results are reported in Figure SM1 in the Supplementary Material section. Two sharp bands at 2172 and 2156 cm^{-1}, assigned to CO adsorbed on two kinds Ce^{4+} sites with different co-ordinative unsaturation [29] and less intense bands at 2125 and 2101 cm^{-1}, due to CO on Au^{0} [30, 31] and on positively charged Au [32], are observed on Ce300Au300 on interaction with 0.25 mbar CO at 90 K. The same experiment carried out on Ce500Au500 gave rise only to an intense band at 2156 cm^{-1} due to CO on Ce^{4+} sites as well as to a weak component at 2101 cm^{-1}, related to CO on gold. The band at 2176 cm^{-1} is totally depleted, therefore the thermal treatment in oxygen at 500 °C strongly changed the population of ceria surface sites:only more coordinated Ce^{4+} sites are exposed at the surface of Ce500Au500. At the same time, a decrease in intensity of the band at 2101 cm^{-1}, due to the presence of a lower amount of Au sites, is observed. No positively

charged gold sites are observed. The exclusive presence of one kind of Ce^{4+} sites, i.e. those responsible of the band at 2156 cm^{-1}, can be related to the enhanced reactivity of Ce500Au500. These features are an indication that some agglomeration of the Au nanoparticles occurred at 500°C, in agreement with our findings. Therefore, the calcination to which the catalyst were submitted after gold dp has an effect on the size of gold nanoparticles and consequently on the catalytic performances, too. In particular, the higher is the final calcination temperature, the lower is the gold dispersion. This effect is more evident when the support is pretreated at 500 °C as confirmed by the HRTEM measurements performed on Ce110Au500 and Ce500Au500 and by the FTIR experiments of adsorbed CO on Ce300Au300 and Ce500Au500 catalysts. Therefore, the final calcination step either at 300 °C or at 500 °C has the effect to guarantee presence of gold particles with a greater size, resulting from the agglomeration of the smaller nanoparticles.

It has been observed that the size of gold has no influence on the selectivity to methylfuroate, that is 100 % for all catalysts. However, the size has a marked effect on the conversion: in particular, the observed increase of the size of gold corresponds to an increase in the catalytic activity. These results appear in sharp contrast with our previous characterization on Au/ZrO_2 catalysts [4, 5, 7]. Indeed, we found that the calcination of Au/ZrO_2 a proper temperature can produce an efficient catalyst for the oxidative esterification of furfural. In particular, it was found that the calcination at 500 °C allowed to modulate gold nanosize (below 3 nm) and above all to stabilize gold clusters, that are able to activate molecular oxygen producing atomic gold species [33], that render the catalyst more active for furfural esterification reaction [4,5].

The characterisation findings reported in the present paper clearly indicate that Au/CeO_2 needs no gold cluster to activate oxygen and to catalyse the reaction. How this apparent incongruence with our previous results can be explained? It has been recently reported that small molecules (CO, NO, etc.) can be activated only on small gold nanoparticles or roughened Au(111) surfaces, i.e. in the presence of considerable disorder, whereas well-ordered Au(111) single crystals or extended metal films are active in the reaction of certain large molecules [34], such as those involved in the 2-FA oxidative esterification reaction. It can be proposed that in reaction conditions ceria is able to provide activated oxygen instead of gold clusters with simultaneous creation of neutral oxygen vacancies, according to the following reaction (in Kröger-Wink notation):

$$O_O^x + 2Ce_{Ce}^x \rightarrow V_O^{\bullet\bullet} + 2Ce_{Ce}^{'} + \tfrac{1}{2} O_2\,(g)$$

In addition, the created oxygen vacancies could further play a role by activating the reactant oxygen molecules coming from the gas phase [35, 36]. Such activation can enhance the reactivity of the Au/CeO_2 system. A more efficient furfural activation by ceria oxygen vacancies could be also hypothesised, basing on our previous spectroscopic results that pointed out that both furfural and methylfuroate interact mainly with their carbonylic group with the surface of the catalyst [7].

We demonstrated recently that methoxy species, possibly bridged on Zr^{4+} and Au sites at the perimeter of the metal nanoparticles close to the support are directly involved in the furfural esterification reaction [7]. The findings revealed that on Au/ZrO_2 catalysts the gold active sites have the dual role to activate oxygen and to host methoxy species involved in the formation of the methylfuroate product.

According to Scheme 2, we propose that ceria can effectively provide activated oxygen instead of gold: these activated oxygen atoms can then spillover from the ceria support to the gold.

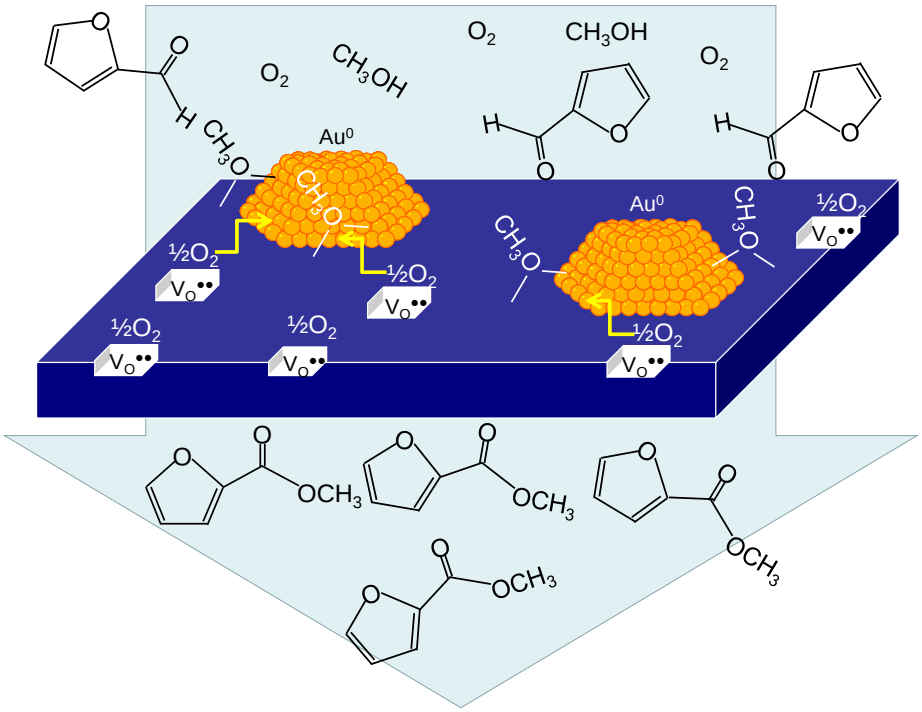

Scheme 2: Proposed role of ceria and of gold nanoparticles in the 2-FA oxidative esterification reaction.

Reverse oxygen spillover involving transport of activated oxygen from ceria to Pt was experimentally detected by resonant photoelectron spectroscopy on Pt/CeO_2 catalysts [37]. Moreover, the authors found that the reverse oxygen spillover occurs at a nanoscale level, being operative mainly on nanostructured ceria supports, such as those investigated in the present study. The same phenomenon was also observed for Ag on CeO_2 (111) thin films, again at the boundary of the metal nanoparticles [38]. We tried

new FTIR experiments to support the possibility of reverse spill over from ceria to Au. More in detail, Ce500Au500 was contacted with methanol and furfural at 120° for 30 min in the absence of oxygen in order to force the oxygen atoms coming from ceria to take part to the reaction as well as to be able to distinguish between oxygen coming from ceria and oxygen coming from the gas phase. The surface of the catalyst was monitored by CO adsorption at 90 K before and after the inlet of the methanol/furfural mixture to probe the nature of the exposed sites and to support our proposal. The results are shown in Figure SM2 in the Supplementary aterial section. As already described, the spectra collected on Ce500Au500 catalyst after CO adsorption at 90 K (section a) reveal the presence of a very intense absorption band with maximum at 2156 cm^{-1} due to CO on Ce^{4+} sites [29] and of a weak band at 2101 cm^{-1}, due to CO on gold sites [30, 31]. On the contrary, a band at 2147 cm^{-1}, due to CO on Ce^{3+} sites [29] and a very weak absorption at 2100 cm^{-1}, related to CO on gold, are observed after contacting the Ce500Au500 with methanol and furfural at 120 °C for 30 min (section b). A broad adsorption at 2135 cm^{-1}, assigned to CO on positively charged gold [32], is still detected upon outgassing at 90 K (blue curve). Moreover, a band at 2340 cm^{-1} related to the asymmetric stretching of CO_2 molecularly adsorbed [39] is observed after the inlet of CO at 90 K, indicating that some residual oxygen adsorbed on gold reacted with the CO probe.

Some weak bands related to the presence of methyl-2-furoate are detected after heating in the methanol/furfural mixture at 120°C for 30 min and cooling at r.t. (section c of Figure S2) [7]. Moreover, the band at 1106 cm^{-1} due to on top methoxy species [27, 28] and formed upon methanol inlet at r.t. is markedly decreased in intensity after heating in methanol/furfural at 120 °C for 30 min, indicating an involvement of methoxy species.

The above findings could be taken as an indication that the oxygen reverse spillover occurred: indeed the ceria surface is reduced, as indicated by the band related to Ce^{3+} sites, and gold is partially oxidised, in agreement with the possibility of reverse spill over. Therefore, the oxygen reverse spillover could make the gold sites located at the perimeter of the Au nanoparticles close to the ceria support able to activate effectively the methanol molecule, similarly to what previously observed by us [7].

4. Conclusions

The results put in evidence the important role played by two different steps in the preparation of the samples:

(i) the temperature to which the support is calcined;

(ii) the final calcination temperature to which the catalyst is submitted after gold dp.

The calcination steps strongly influence the final size of the gold nanoparticles, whilst the ceria support is not apparently modified in size and structure (with the exception of the Ce90 sample). The calcination at 500 °C allowed to obtain gold nanoparticles with greater size if compared to the samples calcined at lower temperature. Unexpectedly, the larger is the size of gold, the higher is the catalytic activity, according to the trend: Ce500Au500> Ce300Au300> Ce110Au500 ~ Ce110Au300 ~ Ce90Au300 > Ce90Au500. On the contrary, no influence on the selectivity to methylfuroate has been detected.

The characterisation results demonstrated that Au/CeO_2 catalysts need no gold cluster to activate oxygen and to catalyse the reaction. The comparison between Ce300Au300 and Ce500Au500 indicated the presence of different amounts of carbonate

species at the surface. The abundance of these species as well as the exclusive presence of more coordinated Ce4+ sites on Ce500Au500 can explain the different catalytic activity displayed by the two systems, being related to the capability of ceria to provide activated oxygen with consequent formation of oxygen vacancies. The cleaner is the ceria surface, the higher is the ability to release oxygen. It has been proposed that reverse oxygen spillover can occur at the perimeter of the nanoparticles and that the role of these gold sites could the activation of methanol molecules at the perimeter of the nanoparticles. Moreover, adsorbed methoxy species are less stable on the surface of Ce500Au500, possibly indicating an enhanced reactivity on this sample.

5. Acknowledgments

We thank Mrs.Tania Fantinel for technical assistance. Financial support to this work by MIUR (Cofin 2008) is gratefully acknowledged.

References

[1] J. C. Serrano-Ruiz, R. Luque, J. H. Clark, in: K. Triantafyllidis, A. Lappas, M. Stocker (Eds.), The role of catalysis for the sustainable production of bio-fuels and bio-chemicals, Elsevier, Amsterdam, 2013, p. 557.

[2] E. Taarning, I. S. Nielsen, K. Egeblad, R. Madsen, C. H. Christensen, ChemSusChem 1 (2008) 75.

[3] O. Casanova, S. Iborra, A. Corma, J. Catal. 265 (2009) 109.

[4] F. Pinna, A. Olivo, V. Trevisan, F. Menegazzo, M. Signoretto, M. Manzoli, F. Boccuzzi, Catal. Today 203 (2013) 196.

[5] M. Signoretto, F. Menegazzo, L. Contessotto, F. Pinna, M. Manzoli, F. Boccuzzi, Appl. Catal. B. 129 (2013) 287.

[6] F. Menegazzo, M. Signoretto, F. Pinna, M. Manzoli, V. Aina, G. Cerrato, F. Boccuzzi, J. Catal. 309 (2014) 241.

[7] F. Menegazzo, T. Fantinel, M. Signoretto, F. Pinna, M. Manzoli, J. Catal. 319 (2014) 61.

[8] P. Dutta, S. Pal, M. S. Seehra, Y. Shi, E. M. Eyring, R. D. Ernst, Chem. Mater. 18 (2006) 5144. •

[9] M. Melchionna, P. Fornasiero, Materials Today 17 (2014) 349.

[10] M. Primet, E. Garbowski, in: A. Trovarelli (Ed.), Catalysis by ceria and related materials, Catalytic Science, vol. 2, Imperial College Press, Singapore, 2002, p. 407.

[11] L. Kundakovic, M. Flytzani-Stephanopoulos, J. Catal. 179 (1998) 203.

[12] F. Menegazzo, P. Burti, M. Signoretto, M. Manzoli, S. Vankova, F. Boccuzzi, F. Pinna, G. Strukul, J. Catal. 257 (2008) 369.

[13] S.J. Gregg, K.S.W. Sing, Adsorption, Surface Area and Porosity – 2nd ed., Academic Press, 1982, p. 111.

[14] F. Menegazzo, F. Pinna, M. Signoretto, V. Trevisan, F. Boccuzzi, A. Chiorino, M. Manzoli, Appl. Catal. A. 356 (2009) 31.

[15] A.A. Ansari, A. Kaushik, J. Semiconductors 31 (2010) 033001/1.

[16] M. Balasubramanian, C.A. Melendres, A.N. Mansour, Thin Solid Films 347 (1999) 178.

[17] J. Hua, Y.Dong, X.Chen, H.Zhang, J.Zheng, Q. Wang, X. Chen, Chem. Eng. J. 236 (2014) 1.

[18] Z.C. Orel, B. Orel, Phys. Status Solidi B, 186 (1994) K33.

[19] H. Kangar, H. Ghazavi, M. Darroudi, Ceramics International, 41 (2015) 4123.

[20] M.I. Zaki, G.A.M. Hussein, S.A.A. Mansour, H.M. Ismail, G.A.H. Mekhemer, Colloids Surfaces A: Physicochem. Eng. Aspects 127 (1997) 47.

[21] M.A. Centeno, M. Paulis, M. Montes, J.A. Odriozola, Appl. Catal. A: General 234 (2002) 65.

[22] E. Kowalska, O.O. Prieto Mahaney, R. Abe, B. Ohtani, Phys. Chem. Chem. Phys. 2010, 12, 2344.

[23] J. Tiggesbaumker, L. Koller, H.O. Lutz, K.H. Meiwesbroer, Chem. Phys. Lett., 190 (1992) 42.

[24] A. Leibsch, Phys. Rev. B: Condens. Matter, 48 (1993) 11317.

[25] A. Moores, F. Goettmann, New J. Chem., 30 (2006) 1121.

[26] C. Binet, M. Daturi, J.-C. Lavalley, Catal. Today 50 (1999) 207.

[27] A. Badri, C. Binet, J.-C. Lavalley, J. Chem. Soc., Faraday Trans. 93 (1997) 1159.

[28] C. Binet, M. Daturi, Catal. Today 70 (2001) 155.

[29] C. Binet, M. Daturi, J.C. Lavalley, Catal. Today 50 (1999) 207.

[30] F. Boccuzzi, A. Chiorino, M. Manzoli, D. Andreeva, T. Tabakova, J. Catal. 188 (1999) 176.

[31] T. Tabakova, F. Boccuzzi, M. Manzoli, D. Andreeva, Appl. Catal. A: General 252 (2003) 385.

[32] M. Manzoli, F. Boccuzzi, A. Chiorino, F. Vindigni, W. Deng, M. Flytzani-Stephanopoulos, J. Catal., 245 (2007), 308.

[33] M. Turner, V.B. Golovko, O.P.H. Vaughan, P. Abdulkin, A. Berenguer-Murcia, M.S. Tikhov, B.F.G. Johnson, R. Lambert, Nature 454 (2008) 981.

[34] L. Guczi, A. Beck, Z. Pászti, Catal. Today 181 (2012) 26.

[35] V.V. Pushkarev, V.I. Kovalchuk, J.L. d'Itri, J. Phys. Chem. B 108 (2004) 5341.

[36] F. Vindigni, M. Manzoli, A. Damin, T. Tabakova, A. Zecchina, Chem. Eur. J. 17 (2011) 4356.

[37] G.N. Vassilov, Y. Lykhach, A. Migani, T. Staudt, G.P. Petrova, N. Tsud, T. Skála, A. Bruix, F. Illas, K.C. Prince, V. Matolín, K.M. Neyman, J. Libuda, Nature Materials, 10 (2011) 310.

[38] D. Kong, G. Wang, Y. Pan, S. Hu, J. Hou, H. Pan, C.T. Campbell, J. Zhu, J. Phys. Chem. C 115 (2011) 6715.

[39] F. Boccuzzi, A. Chiorino, M. Manzoli, P. Lu, T. Akita, S. Ichikawa, M. Haruta, J. Catal. 202 (2001) 256.

Captions

Figure 1: TG-DTA analysis of the Ce110 support.

Figure 2: XRD patterns of the different ceria supports.

Scheme 1: Oxidative esterification of furfural to methyl-2-furoate.

Figure 3: Catalytic performances in the 2-FA oxidative esterification for the examined samples. Selectivity is 100% for all catalysts. (at 120 °C - 6 bar O_2 – 90 min of reaction).

Table 1: Characterization data of the catalysts.

Figure 4: N_2 physisorption isotherms of the catalysts and BHJ pore size distributions (insert).

Figure 5: X-ray diffraction patterns of the catalysts prepared by dp. Inset: zoom of the XRD pattern of Ce500Au500 in the 30-45 2 θ range.

Figure 6: HRTEM images collected on Ce110Au500 (section a) and Ce500Au500 (sections c and d): roundish Au nanoparticles with different size are signaled by orange and red circles, respectively. The Au particle size distributions of Ce110Au500 (orange) and Ce500Au500 (red) are reported and compared in section b. Instrumental magnification: 300000X, 400000X and 500000X, respectively.

Figure 7: DRUV-Vis spectra of the as prepared samples supported on ceria.

Table 2: DRUV-Vis and CO chemisorption data of the catalysts

Figure 8: CeO_2 particle size distributions of Ce110Au500 (orange) and Ce500Au500 (purple).

Figure 9: FTIR absorbance spectra of Ce300Au300 (orange curves) and Ce500Au500 (blue curves) outgassed at r.t. 30’ (section a) and after oxidation at 300 °C and 500 °C, respectively (section b).

Figure 10. FTIR difference spectra collected on Ce300Au300 (section a) and Ce500Au500 (section b) upon the inlet of 5 mbar CH_3OH (red curves) and under outgassing at r.t. after 1' (orange curves), after 10 min (brown curves), after 30' (blue curves).

Scheme 2: Proposed role of ceria and of gold nanoparticles in the 2-FA oxidative esterification reaction.

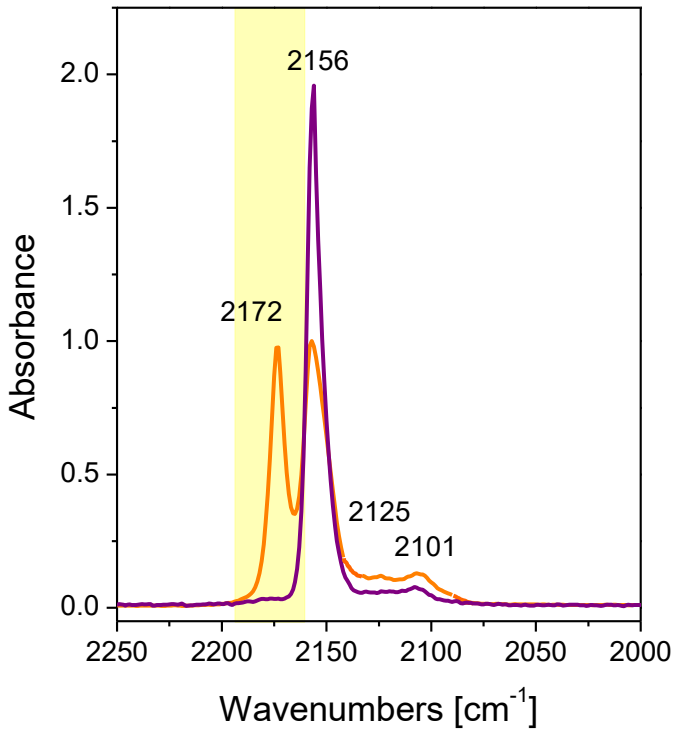

Figure SM1: FTIR absorbance spectra of 0.25 mbar CO adsorbed at 90 K on Ce300Au300 treated in O_2 at 300°C (orange curve) and on Ce500Au500 treated in O_2 at 500°C (violet curve).

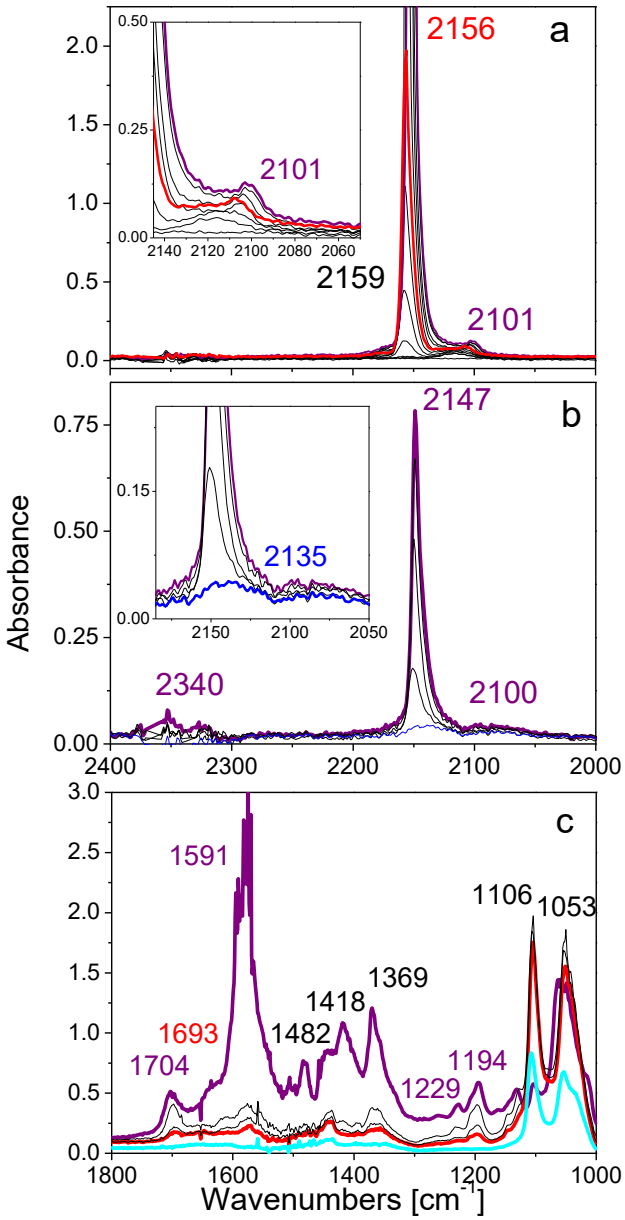

Figure SM2: Section a: FTIR absorbance spectra of 4.5 mbar CO adsorbed at 90 K (violet curve), at decreasing pressures and after outgassing at the same temperature (black and red curves) on Ce500Au500 treated in O_2 at 500°C. Section b: FTIR absorbance spectra of 4.5 mbar CO adsorbed at 90 K (violet curve), at decreasing CO pressures (black curves) and after outgassing at the same temperature (blue curve) on Ce500Au500 after reaction. Insets: zoom on the 2145-2050 cm^{-1} range. Section c: FTIR absorbance spectra of 0.5 mbar CH_3OH adsorbed at r.t. (cyan curve), after subsequent inlets of furfural (red and black curves) on preadsorbed methanol at r.t. and after heating the mixture at 120°C for 30 min and cooling to r.t..